CAECENET: An automatic system processing photometer and ceilometer data from different networks to provide columnar and vertically-resolved aerosol properties

Celia Herrero del Barrio[1], Roberto Román[1], Ramiro González[1], Alberto Cazorla[2,3], Marcos Herreras-Giralda[4], Juan Carlos Antuña-Sánchez[1,4], Francisco Molero[5], Francisco Navas-Guzmán[2,3], Antonio Serrano[6], María Ángeles Obregón[6], Yolanda Sola[7], Marco Pandolfi[8], Sara Herrero-Anta[1], Daniel González-Fernández[1], Jorge Muñiz-Rosado[2,3], David Mateos[1], Abel Calle[1], Carlos Toledano[1], Victoria E. Cachorro[1], and Ángel de Frutos[1]

[1]Group of Atmospheric Optics (GOA-UVa), Universidad de Valladolid, 47011, Valladolid, Spain
[2]Department of Applied Physics, Universidad de Granada, 18071, Granada, Spain
[3]Andalusian Institute for Earth System Research, IISTA-CEAMA, Granada, Spain
[4]GRASP-SAS, Remote Sensing Developments, Villeneuve D'Ascq, France
[5]Departamento de Medio Ambiente, Centro de Investigaciones Energéticas, Medioambientales y Tecnológicas (CIEMAT), 28040 Madrid, Spain
[6]Departamento de Física, Universidad de Extremadura, Badajoz, Spain
[7]Group of Meteorology, Department of Applied Physics, Faculty of Physics, Universitat de Barcelona, Barcelona, Spain
[8]Institute of Environmental Assessment and Water Research (IDAEA-CSIC), Barcelona, Spain

Correspondence: Celia Herrero del Barrio (celia@goa.uva.es)

Abstract. This work introduces CAECENET, a new system capable of automatically retrieving columnar and vertically-resolved aerosol properties running the GRASP (Generalized Retrieval of Atmosphere and Surface Properties) algorithm using sun-sky photometer (aerosol optical depth, AOD; and sky radiance measurements) and ceilometer (range corrected signal; RCS) data as input. This method, so called $GRASP_{pac}$, is implemented in CAECENET, which assimilates sun-sky photometers data from CÆLIS database and ceilometer data from ICENET database (Iberian Ceilometer Network). CAECENET allows for continuous and near-real-time monitoring of both vertical and columnar aerosol properties. The main characteristics and workflow of CAECENET are explained in detail. This work also explores the potential of CAECENET to monitor and analyze the evolution of transported aerosol events on a regional scale by means of the distribution of CAECENET stations across the Iberian Peninsula. As an example, this paper analyzes, using the CAECENET products, the case of a Saharan dust outbreak that occurred between the 3rd and 5th of October 2022. This was an intense event, with AOD at 440 nm values around 0.5 in Madrid and Valladolid, and reaching 1.55 in Granada. Transport from the Canadian wildfires at the end of June 2023 is also studied. Despite the long-range transport of the smoke particles in this event, measured volume concentrations reached and surpassed 80 $\mu m^3/\mu m^2$ in some stations. The results obtained point to the utility of this CAECENET tool for analyzing changes in the height and speed of the event propagation, in the aerosol concentration, and how this affects the optical properties.

1   Introduction

The knowledge of the columnar and vertically-resolved atmospheric aerosol properties is crucial for climate studies, as well as for other fields like aviation or air quality, among others. Moreover, monitoring these properties in near real time is important for making early decisions about air quality and pollution, air traffic, and for the demand of information by the general public.

Sun-sky photometers, which measure solar irradiance and sky radiances at different wavelengths, are frequently used to retrieve aerosol properties such as aerosol optical depth (AOD) in the atmospheric column. These automatic instruments are used as reference instrument by some worldwide networks, such as AERONET (AErosol RObotic NETwork; Holben et al., 1998), to provide advanced aerosol properties in the atmospheric column in near-real-time (NRT) (Giles et al., 2019; Sinyuk et al., 2020). A part of the AERONET photometers is managed by the Group of Atmospheric Optics from the University of Valladolid (GOA-UVa). To carry out this management task, the GOA-UVa developed the CÆLIS software tool (Fuertes et al., 2018), which receives the photometer data and processes them to generate products like AOD (González et al., 2020 a).

Measures of AOD and sky radiances from sun-sky photometers are generally used together in inversion codes to retrieve advanced columnar aerosol properties like volume size distribution and the complex aerosol refractive index (Dubovik and King, 2000; Dubovik et al., 2000, 2006), but without vertical resolution. On the other hand, lidars are generally used for the retrieval of vertically-resolved profiles of aerosol properties like aerosol backscattering (Klett, 1981, 1985; Fernald, 1984; Sasano and Nakane, 1984) and extinction coefficients (Ansmann et al., 1990; Whiteman et al., 1992). In this sense, some networks like EARLINET (Pappalardo et al., 2014) and PollyNET (https://polly.tropos.de) manage multi-wavelength lidar data to provide some aerosol products. However, these lidars are usually expensive and not fully automatic, and there is a scarce supply of this kind of instrument. A cheaper alternative to lidars are ceilometers and single-wavelength lidars, which are fully automatic measuring continuously at one single wavelength. The amount of these low power instruments around the world is much higher. In this sense, there are networks providing ceilometer products in NRT, such as the automatic lidars and ceilometers (ALC) network, which is part of E-PROFILE (https://ceilometer.e-profile.eu), and the Iberian Ceilometer Network (ICENET; Cazorla et al., 2017).

To obtain advanced aerosol properties similar to those with sun-sky photometer but vertically resolved, Román et al. (2018) developed the $GRASP_{pac}$ method, which combines sun-sky photometer and ceilometer measurements into GRASP code (Generalized Retrieval of Atmosphere and Surface Properties; Dubovik et al., 2014, 2021) retrieving geometric vertical and columnar aerosol properties. This method can be applied to exploit the high amount of data from collocated sun-sky photometers and ceilometers. In fact, the $GRASP_{pac}$ method has been already used to retrieve and analyze vertical aerosol properties in some stations like high-mountain locations (Titos et al., 2019; Herreras et al., 2019). However, in these cases, the aerosol products were manually processed, not in NRT, to carry out these specific studies. In this sense, the availability in near-real time of $GRASP_{pac}$ products automatically processed can be useful to exploit synergies between these instruments since it is possible to constantly monitor vertically-resolved aerosol properties and update the results derived from the aforementioned studies.

In this framework, the main objective of this work is to develop and establish a system capable of assimilation of data from sun-sky photometer and ceilometer networks to apply the $GRASP_{pac}$ method and provide NRT vertically resolved and

columnar aerosol properties. Databases used to this end are CÆLIS for AOD and sky radiances (sun-sky photometer data) and

50 ICENET for the ceilometer range corrected signal (RCS) data. The combination of both databases (CÆLIS and ICENET) is what gives the developed system its name: CAECENET. The use of CAECENET products for climate studies and the analysis of regional aerosol events is also among the goals of this work in order to test the capability of this new tool.

This paper is structured as follows: Section 2 describes the CAECENET system, its main characteristics, structure, and workflow; Section 3 presents the detailed analysis of two aerosol events over the Iberian Peninsula using CAECENET products;

55 finally, Section 4 summarizes the main conclusions of this work.

2 Instruments and Data processing

CAECENET is a system that has implemented the automatic application of the GRASP$_{pac}$ method using sun-sky photometer and ceilometer data. All these data are obtained directly from CÆLIS and ICENET databases, respectively, which are explained in the next subsections.

60 ### 2.1 CÆLIS and photometer data

The CE318 sun-sky photometer (*Cimel Electronique*) is the main instrument of AERONET. It is basically formed by a head with one Silicon and one InGaAs sensor with a filter wheel and a collimator tube, that measures at several wavelengths (generally 340, 380, 440, 500, 675, 870, 940, 1020 and 1640 nm) the Sun direct irradiance and the sky radiance at different sky angles thanks to a 2 axis robot. A recent model (CE318-T) also allows lunar irradiance measurements to derive the AOD at

65 night-time (Barreto et al., 2013, 2016, 2017; Román et al., 2017, 2020). This new model is also capable to performance the sky radiance measurements in three different geometries: Almucantar, where the zenith angle is equal to solar zenith angle and the measurements are done for different sky azimuth angles; Principal Plane, where the azimuth angle is equal to the solar azimuth angle and the measurements are carried out for different sky zenith angles; and Hybrid, which is a combination of Almucantar and Principal Plane. More information about these sky radiance scenarios can be found in Sinyuk et al. (2020).

70 CÆLIS is a web tool developed by the GOA-UVa with the main goal of managing the calibration and quality control of the AERONET photometers that the calibration center at Valladolid is in charge of. CÆLIS, based on a client-server architecture, is composed of three main modules: 1) a relational database to store the raw photometer measurements of each instrument, but also the ancillary data needed for the retrieved products, such as optical depth from different gases or climatology values of the Bidirection Reflectance Distribution Function (BRDF); 2) a web interface that allows the monitoring of the performance of all

75 different instruments; and 3) a processing chain that provides products, such as AOD and sky radiances, in NRT. These three modules are explained in detail in Fuertes et al. (2018).

The processing chain of CÆLIS starts when a raw data file from a photometer is received in the server, activating a set of triggers in the NRT module. The NRT module processes the data to retrieve products but also assimilates the needed ancillary data, which are used to compute the AOD and sky radiances (González et al., 2020 a). There are two levels of data for AOD,

80 level 1.0 for all measurements even contaminated by clouds, and level 1.5, where the data are cloud screened following the criteria explained in González et al. (2020 a) based on Giles et al. (2019).

2.2 ICENET and ceilometer data

The Iberian Ceilometer Network (ICENET) is an initiative of the Atmospheric Physics Group of the University of Granada for the coordination and validation of ceilometer measurements at a regional scale. The main goal of ICENET is obtaining reliable
85 vertically resolved aerosol properties in near real time (Cazorla et al., 2017).

Currently, five stations are operating in NRT and another four stations had provided data in the past or intermittently. Figure 1 shows the spatial distribution of the stations.

The main instrument in ICENET is the Lufft CHM15k-Nimbus ceilometer. This ceilometer operates with a pulsed Nd:YAG laser emitting at 1064 nm and has vertical resolution of 15 m. The vertical range expands from 15 to 15360 m. The instrument
90 has its own overlap correction and for all instruments in ICENET, the overlap function provided by the manufacturer shows an overlap over 90% between 555 and 885 m a.g.l. Most stations also have a collocated sun-sky photometer from AERONET and AOD information is used as ancillary information for the calibration and inversion modules explained bellow.

ICENET operates with several modules:

- The acquisition module obtains data from the ceilometers and organizes them in the corresponding dataset. AERONET
95   data is also obtained for those stations with collocated sun-sky photometer.

- The calibration module calibrates the RCS following the procedure described by Cazorla et al. (2017) and provides attenuated backscatter coefficient.

- The inversion module provides backscattering coefficient and extinction coefficient applying the Klett-Fernald inversion (Klett, 1981, 1985) to the RCS.

100 - The CAECENET module prepares the RCS signal from the ceilometers in the adequate format for the $GRASP_{pac}$ retrieval and sends it to CAECENET (see next section).

All these modules can operate in NRT for connected stations that provide ceilometer data. For non-connected stations or for case studies, manual operation is also possible.

2.3 $GRASP_{pac}$ retrieval

105 The GRASP algorithm is a versatile inversion code capable to retrieve atmospheric and surface properties properties, among others, using different sets of observations. This code is based on multi-term least square method (Dubovik and King, 2000) but its flexibility allows the stand-alone inversion of the measurements of different instruments like: satellite instruments (Chen et al., 2020; Wei et al., 2021), sun-sky photometers (Torres et al., 2017; Torres and Fuertes, 2021; Molero et al., 2020), lidars (Lopatin et al., 2021), sky cameras (Román et al., 2022), polar nephelometers (Espinosa et al., 2017) or zenithal radiometers
110 (Herrero-Anta et al., 2023), among others; but also the joint inversion of combined measurements from different instruments,
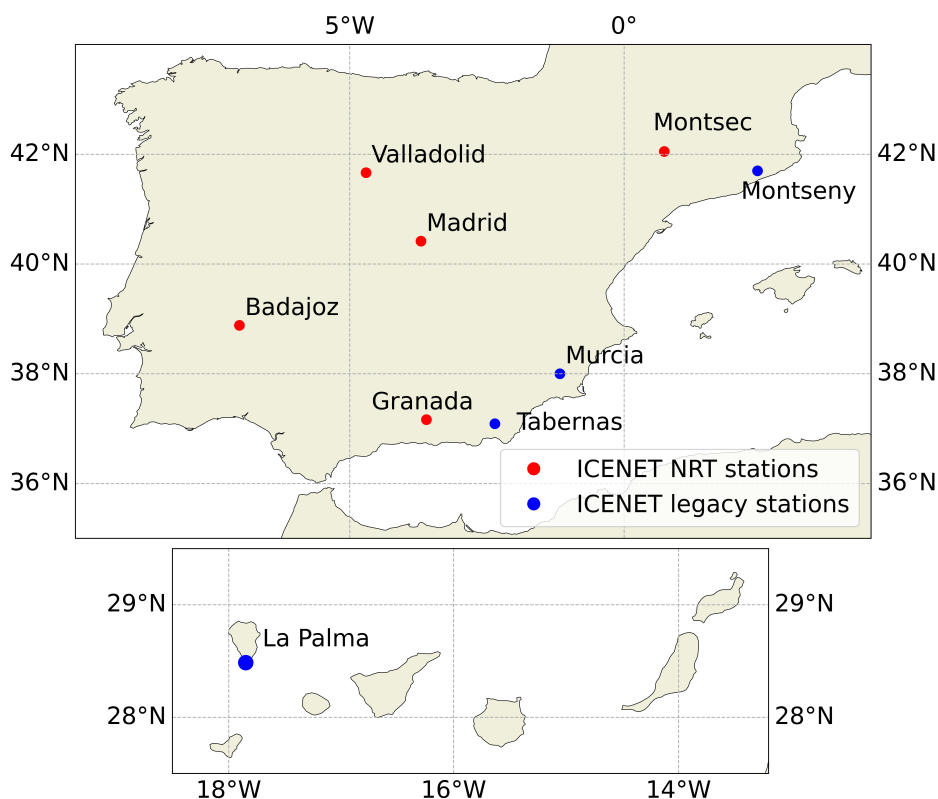
Figure 1. Map of the Iberian Peninsula, including the Canary and Balearic islands, showing the location of ICENET stations. Red dots represent the ceilometers operating in near-real-time conditions while blue dots correspond to legacy stations providing data in the past or intermittently.

such as sun-sky photometers plus lidars (Lopatin et al., 2013; Benavent-Oltra et al., 2017; Tsekeri et al., 2017) or plus sky cameras (Román et al., 2017; Benavent-Oltra et al., 2019).

One of the inversion strategies developed for GRASP is the so called GRASP$_{pac}$ (*pac* is the acronym of *photometer and ceilometer*), which combines AOD and sky radiance measurements from sun-sky photometer with RCS data from ceilometer. The GRASP$_{pac}$ method uses as input the measurements of AOD and sky radiances at 440, 675, 870 and 1020 nm from photometers, and the measured RCS at 1064 nm from ceilometer. Each GRASP$_{pac}$ retrieval is centered in time for the sky radiance measurements, which can be performed under Almucantar or Hybrid scenarios. These sky radiances are previously filtered by clouds assuming that measurements performed under symmetric scattering angles must show differences below 20% between both branches. A GRASP$_{pac}$ retrieval is not performed if there are not more than 10 sky radiance values per wavelength and at least one measurement in four different scattering angle ranges (3.2° to 6°, 6° to 30°, 30° to 80° and 80° to 180°). The AOD (cloud-screened) closest in time data to the sky radiance values within ± 16 min are used in the process. Regarding RCS, it is firstly cloud-screened and averaged over a ± 15 min window centered around the sky radiance time. The

5

time averaged RCS undergoes vertical smoothing through a moving average with a window of ± 105 m to mitigate noise. Subsequently, it is normalized across 60 log-spaced bins at various heights, following the approach outlined by Lopatin et al. (2013); the height range for normalization spans from a minimum of 250 m a.g.l. to a dynamic maximum which is usually about 7000 m a.g.l.. The determination of this dynamic maximum and the normalization process is well described by Román et al. (2018). In addition, GRASP$_{pac}$ needs to introduce in GRASP the BRDF, which is modeled by the three parameters of the Li–Ross model (Ross and Ross, 1981; Li and Strahler, 1992)

Regarding the inversion strategy, GRASP$_{pac}$ method approaches the aerosol volume size distribution to a log-space 22 triangle bins distribution with radius from 0.05 to 15 μm without discerning between fine and coarse modes intensive properties; the real and imaginary parts of refractive index are considered as wavelength dependent; and the sphericity, which quantifies the portion of spherical particles and spheroids, is also retrieved. The intensive aerosol properties, like complex refractive index or the shape of volume size distribution, are assumed invariant with height; However, extensive aerosol properties, like aerosol volume concentration (VC) or extinction coefficients, are assumed as height-dependent. The variations of volume size distribution with radius, complex refractive index with wavelength, and aerosol vertical distribution with height, are constrained to be smooth. An *a priori* constraint (Dubovik et al., 2021) is also used for the smoothness of the volume size distribution in GRASP$_{pac}$ method.

As a result, GRASP provides different columnar and vertically-resolved aerosol products. In column: one value of sphericity; the volume size distribution (normalized by particle volume concentration) at 22 radius bins and the total aerosol volume concentration; and five values (one per wavelength) of the real and imaginary parts of the refractive index, the phase function, and other derived products like lidar ratio, single scattering albedo (SSA) and AOD. Regarding vertical properties, GRASP provides the aerosol normalized vertical profile (AVP) at the chosen 60 heights and at ground level, which AVP value is assumed equal to the obtained at the closest height level. The AVP data represents the normalized vertical aerosol concentration, which is used to derive some aerosol extensive properties like profiles of aerosol volume concentration and extinction coefficient, multiplying AVP by total columnar volume concentration and AOD, respectively. Profiles of aerosol scattering coefficient are derived by multiplying extinction by SSA; absorption coefficient profiles as the substraction of extinction minus scattering coefficients; and profiles of backscattering coefficient multiplying the extinction coefficient by lidar ratio.

Furthermore, GRASP counts with its own methodology to calculate the columnar effective radius, volume concentration, and AOD for fine and coarse modes separately. Subsequently, vertical profiles of extinction coefficient and other properties can be computed for the five wavelengths and for the fine and coarse modes separately. However, the shape of these profiles remains equal across all wavelengths and for both modes, following the shape of AVP, since the RCS is only available for one wavelength, preventing the differentiation between fine and coarse particles. Consequently, AVP cannot be determined separately for fine and coarse modes, as observed in multi-wavelength lidar retrievals. As a result, intensive properties such as the Angström Exponent (AE) and the fine/coarse fraction do not exhibit variations with height, even when the profiles of different properties like extinction coefficient are available for different wavelengths and modes.

2.4 CAECENET structure and workflow

As mentioned, CAECENET is a system that has been created to run automatically the GRASP$_{pac}$ method using the sun-sky photometer and ceilometer data from CÆLIS and ICENET as input (Román et al., 2021). CAECENET has been developed as a system with three different main modules: NRT module, database and viewer.

160 Regarding the NRT module, it is responsible for obtaining and merging in one input file the AOD and sky radiances from CÆLIS and the RCS vertical profiles from ICENET and run GRASP code with the GRASP$_{pac}$ configuration. The workflow of this CAECENET task can be shown in Figure 2. The blue lines on this diagram describe the workflow of the CAECENET main algorithm and the red lines all those sub-modules of the algorithm where data from different databases (CÆLIS and ICENET) are consulted. First of all CAECENET looks for new sky radiance observations in CÆLIS database. If there is a new

165 sky radiance measurement (Almucantar or Hybrid), then CAECENET looks for RCS vertical profiles provided by ICENET. If the RCS data passes the quality-assurance and cloud-screening criteria, then the RCS data is averaged to 60 log-spaced points and CAECENET looks for the AOD level 1.5 (cloud-screened) in CÆLIS database. If the AOD is available, the sky radiance measurements are checked, and if they pass the mentioned cloud-screening and quality assurance criteria (i.e., they are invertible), then these radiances are normalized following the GRASP format. This normalization takes into account the

170 measured spectral response of each filter in each sun-sky photometer convoluted by the extraterrestrial spectrum *2000 ASTM Standard Extraterrestrial Spectrum Reference E-490-00* (http://rredc.nrel.gov/solar/spectra/am0.)

All these input values are written for each scenario in a SDATA (Sensor Data) file, following the working methodology of GRASP code. This algorithm needs, to make a retrieval, a SDATA file with the input data, but also a SETTINGS file where the inversion strategy and approaches are included. Then, once the SDATA is obtained, GRASP (version 1.0.1) is run. For this task,

175 CAECENET also modifies the SETTINGS introducing the BRDF values obtained from CÆLIS (climatology tables of V005 Collection MCD43C1 product: V005 MODIS Terra+Aqua BRDF/Albedo 16-Day L3 0.05Deg CMG) and the initial guess values of the size distribution for the chosen scenario. This initial guess depends on the AOD at 440 nm value, as explained by Román et al. (2018).

If there is no cloud-free data of RCS, or AOD level 1.5, or cloud-free sky radiances, then GRASP$_{pac}$ is not run and

180 CAECENET will look for another one. After each retrieval, the output is stored in a file. The NRT module also allows the manager of the system to run or stop NRT for all CAECENET sites and also can be used to reprocess data from the past.

The main results of the GRASP$_{pac}$ output files are also stored into the CAECENET database by the database module. CAECENET has been built based on a relational database to make all the information available for different users and provide a search system. The schema of the used database is simple and scalable, since it stores the output of the GRASP$_{pac}$ retrievals,

185 explained above, discerning four categories: vertical profile properties, optical columnar properties (which also includes asymmetry parameter derived from phase function), microphysical columnar properties and internal status. The data structure of those four categories is different, taking into account the peculiarities of the outputs, as has been explained in the previous subsection.
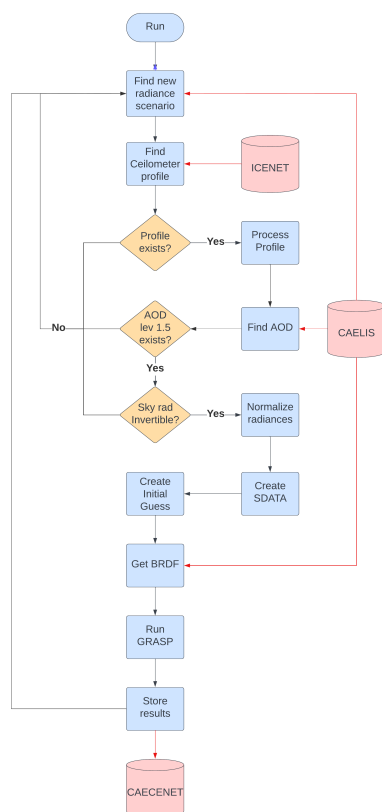
**Figure 2.** Workflow of the CAECENET algorithm.

Finally, to visualize the data produced by CAECENET exits the third main module, a desktop application that acts as a
190   viewer. This viewer allows the users to visualize the data at any station (Román et al., 2021). The output errors are provided as
well, obtaining the ± error interval for each retrieved parameter (Herrera et al., 2022).

3   Results

3.1   Regional dust aerosol event

A high aerosol load event that occurred in the Iberian Peninsula in early October 2022 has been identified and regionally
195   analyzed using CAECENET tool. Data for these days is available for the Granada, Madrid, and Valladolid stations. Figure 3
shows the time series for AOD level 1.5 measurements at 440 and 1020 nm and AE (calculated with all the channels between
440 and 870 nm) provided by CÆLIS. On October 3rd there was a strong increase in the AOD values, compared to the previous
days (<0.1 at all sites), reaching a maximum value of 1.55 at 440 nm in Granada around 13:00 UTC. In Valladolid and Madrid
sites, the AOD values on that day were about 0.5, above the typical values for these stations in central Iberian Peninsula (Mateos
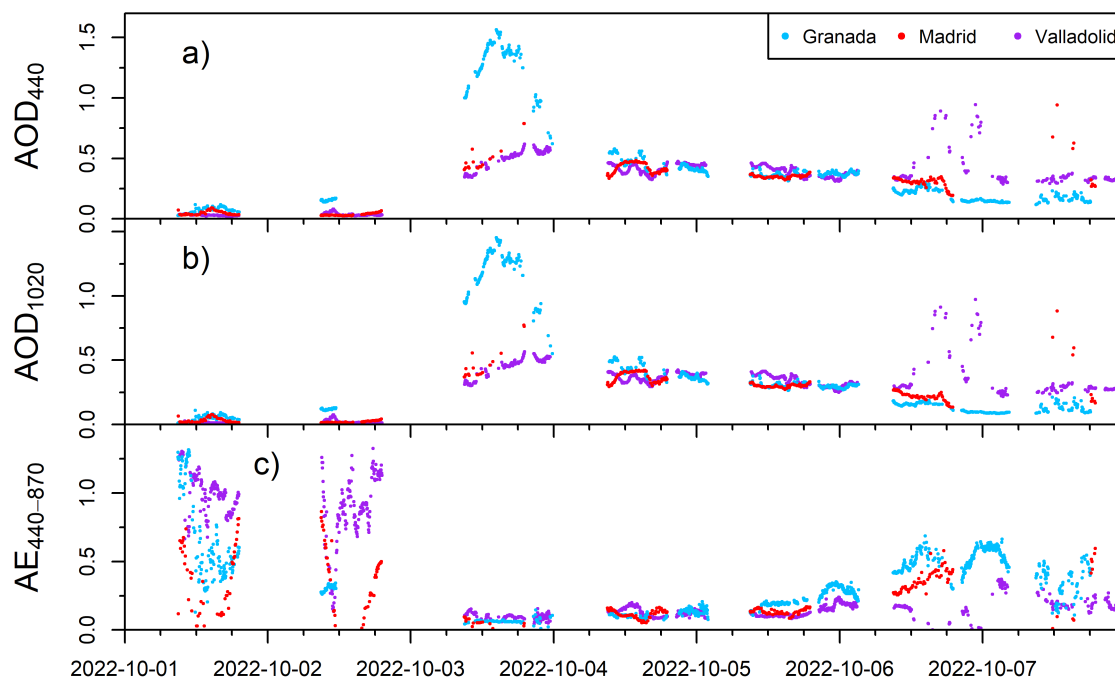
Figure 3. AOD values at 440 nm a), 1020 nm b), and Angström Exponent (AE) c), provided by CÆLIS (level 1.5), for Granada, Madrid and Valladolid stations from October 1st to October 7th, 2022.

et al., 2015). Specifically, the maximum AOD value at 440 nm in Valladolid and Madrid were 0.62 and 0.77, respectively, both around 17:00 UTC. The AOD values at 1020 nm (Figure 3b) were very similar to those at 440 nm for the three stations on 3rd October, implying low spectral dependence on AOD and therefore AE values below 0.2 as observed in Figure 3c for the three locations, indicating that the aerosol particles were mainly coarse. This is a first indicator of a Saharan desert dust outbreak, which fits with other reported events detected in the region (e.g., Cachorro et al., 1987; Toledano et al., 2007; Guerrero-Rascado et al., 2010; Cachorro et al., 2016; Burgos et al., 2016). The AOD values were still about 0.5 with low AE values during 4th and 5th October for the three locations, pointing out the remaining presence of coarse particles. The AE started to increase at the beginning of the night from 5th to 6th October, as can be seen for Valladolid and Granada where a sun-sky-moon photometer (CE318-T) was available. Finally, the AOD on 6th October decreased, particularly for Madrid and Granada, with higher AE values than the previous days, which indicates the end of the coarse-mode dominated event. High AOD values in Valladolid are observed during October 6th but they were most likely caused by the presence of high-altitude clouds such as cirrus (which has been confirmed in images from a sky camera installed at Valladolid).

Figure 4 shows the aerosol volume size distribution (panel a) and the SSA (panel b) for the CAECENET retrieval with the highest AOD value on 3rd October. The highest volume concentration, with values of approximately 0.86 $\mu m^3/\mu m^2$ in Granada
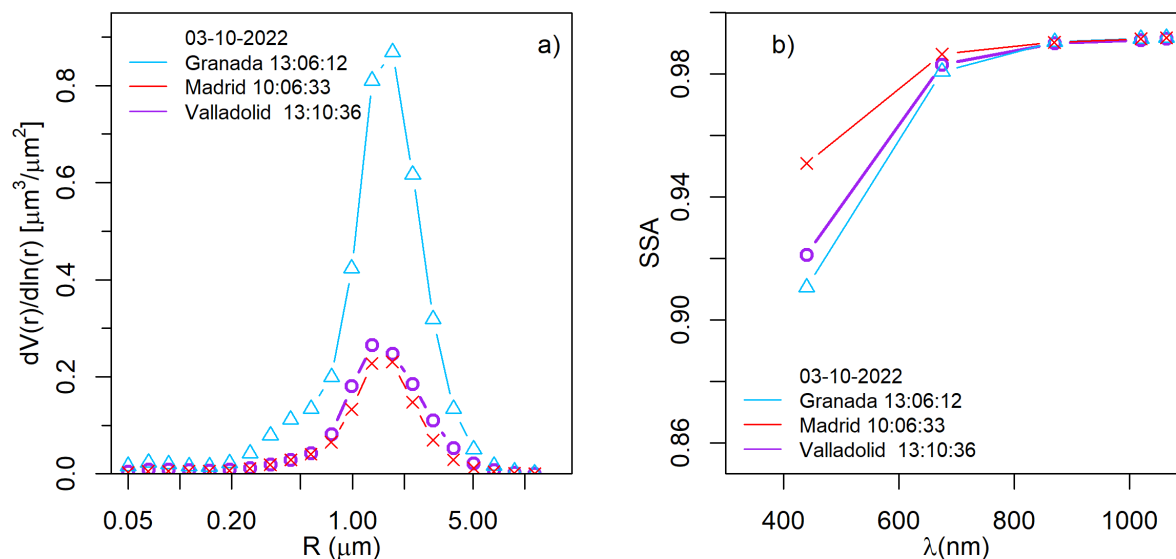
Figure 4. Volume size distribution a) and single scattering albedo (SSA) b) obtained with $GRASP_{pac}$ and provided by CAECENET for the maximum aerosol load reached on 3rd October at Granada, Madrid, and Valladolid.

and about 0.26 μm^3/μm^2 and 0.23 μm^3/μm^2 at Valladolid and Madrid, respectively, appears for a particle radius about 2.25
215   μm in the three stations. It reveals a clear presence of coarse mode, while fine mode is negligible. The SSA, shown in Figure 4b), is above 0.98 for 675 nm to 1020 nm, pointing out that the light absorption of the present aerosol was very low at these wavelengths for the three sites. However, the absorption is higher at 440 nm, especially for Valladolid and Granada where SSA values were about 0.92 and 0.91 at this wavelength. The observed characteristic of size distribution (coarse particles) and SSA values (very low absorption except for the shortest wavelengths) fit with those expected for Saharan dust aerosols (Dubovik
220   et al., 2002; Valenzuela et al., 2015; Burgos et al., 2016).

    The time series of the ceilometer RCS at each station is shown in Figure 5 to qualitatively determine the altitude reached by the aerosol particles during this event. On October 3rd in Granada, a substantial aerosol layer is observed at a very low altitude, ranging from the surface up to 2 km asl and persisted until the afternoon. The aerosol load in this layer seems to be high (the values are above the chosen maximum value in the colorbar legend) which is in line with AOD values about 1.5
225   mentioned above; this layer disappeared at late afternoon when the AOD started to decrease and other aerosol layer appeared between 2 and 4 km asl. A higher aerosol layer, between 2 and 3 km asl arrived in Madrid and Valladolid at the beginning of the same day. These layers persisted throughout the day and became thinner at the end of the day. Figure 5 also shows a high presence of high-altitude clouds in Madrid on 3rd October, which are the main responsible for the scarcity of cloud-screened AOD data on that day. On October 4th, there is a slight decrease in aerosol load and a progressive reduction in altitude of the
230   layer. Two decoupled aerosol layers can be observed around midday in Madrid and Valladolid, later the aerosol appears to be
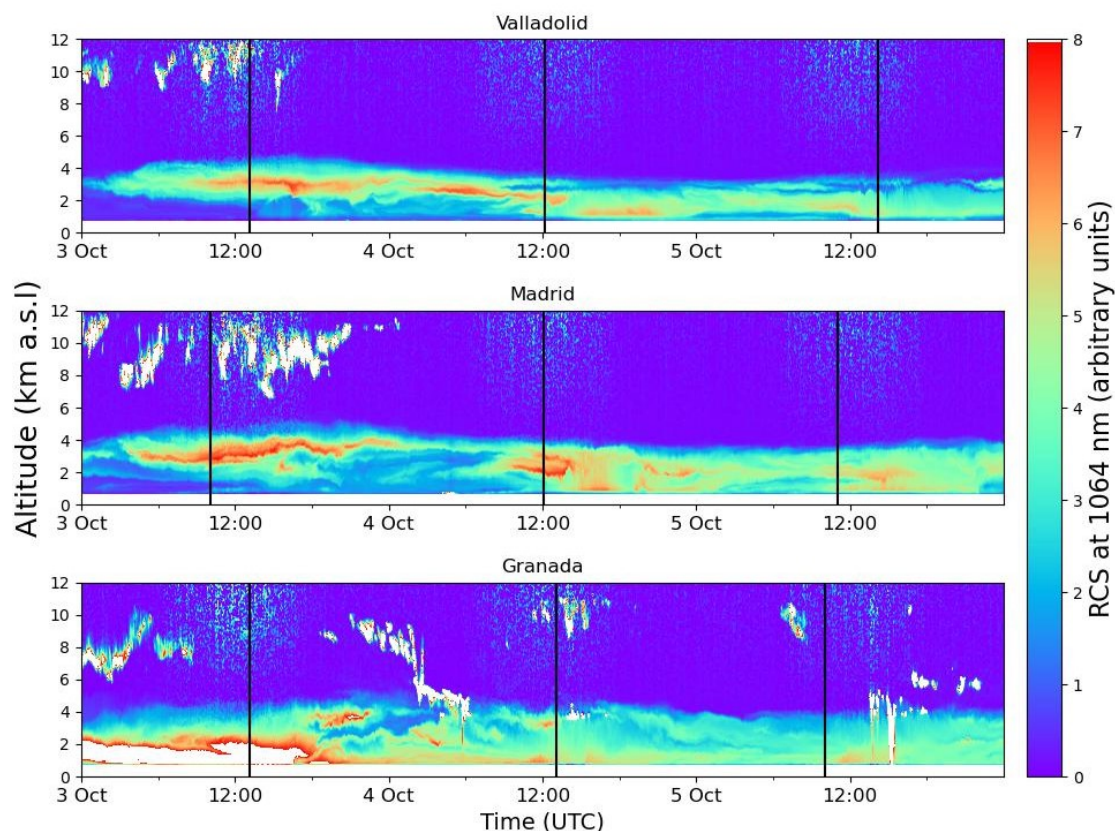
Figure 5. Ceilometer time series of range corrected signal representing the evolution of the dust outbreak between 3 and 5 October 2022 at the stations of Granada (680 m), Madrid (669 m) and Valladolid (705 m). Black vertical lines indicate the time of the profiles in Figure 6 for each station.

mixed within the planetary boundary layer. By October 5th, it is observed that the aerosol load continues to decrease, with the layer remaining below 4 km asl, with the main part near the surface. In addition, some rain precipitation occurred between 14:00 and 15:00 UTC in Granada that could contribute to the wet deposition of aerosol particles.

For a more quantitative characterization, Figure 6 presents vertical volume concentration profiles, obtained from CAECENET, between October 3rd and 5th . The chosen profiles correspond to the available retrievals with the highest AOD value on each day, which are expected to exhibit the highest volume concentrations. On October 3rd, there was a strong aerosol volume concentration in Granada between 1.5 and 4 km asl with values between 250 and 325 μm^3/μm^2. The volume concentration in Madrid and Valladolid presented different behavior than in Granada, which could be attributed to the higher distance and the orography between southern and central Spain. The VC profiles in the other two stations were similar, being mainly distributed in a 2 km width layer centered around 3 km asl with the maximum values about 130 and 180 μm^3/μm^2 in Madrid and Valladolid, respectively. The split of the mentioned aerosol layer in two decoupled aerosol layers can be observed the next day
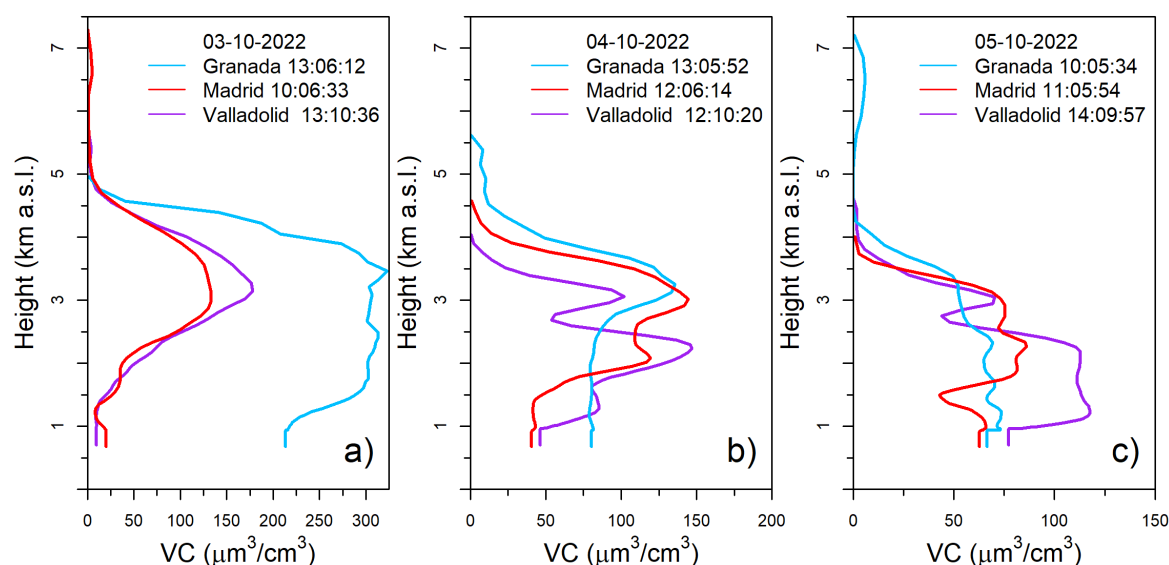
Figure 6. Volume concentration (VC) vertical profiles (altitudes from 0 to 8 km above sea level) at the studied stations. In panel a), the values are shown for October 3rd, in panel b) for the 4th, and in panel c) for the 5th of October 2022, at the hours (UTC) indicated in the legend for each station.

centred at 2 and 3 km asl with the highest value close to 150 $\mu m^3/\mu m^2$ in both stations. This day, a layer also around 3 km asl, but not at 2 km asl, also appeared at Granada with a similar VC values than in Madrid. Finally, on 5th October, the layer structures were no so evident and the peaks of VC appeared in lower heights and with lower values, (below 125 $\mu m^3/\mu m^2$, 90

245   $\mu m^3/\mu m^2$ and 75 $\mu m^3/\mu m^2$ for Valladolid, Madrid and Granada, respectively).

The vertical profiles of the extinction, scattering, absorption, and backscattering coefficients are also available from CAECENET for the days of the event (shown in the appendix). The absorption coefficient values were low, as expected from desert dust particles, for 440 nm wavelength, being lower than 10 Mm^{-1} for Madrid, less than 30 Mm^{-1} for Valladolid and 45 Mm^{-1} for Granada. The scattering coefficient at 440 nm, reached values about 200 Mm^{-1}, 240 Mm^{-1} and 430 Mm^{-1} for Madrid,

250   Valladolid and Granada, respectively. The backscattering coefficient presented values lower than 10 $Mm^{-1}sr^{-1}$ at 440 nm for all three stations and, finally, the extinction coefficient presented values slightly exceeding the scattering coefficient, at 440 nm. The maximum value at Valladolid was 265 Mm^{-1}, 205 Mm^{-1} for Madrid and 469 Mm^{-1} at Granada.

All the results point out that the aerosol type is Saharan dust. To corroborate the origin source of these particles, the HYSPLIT (Hybrid Single-Particle Lagrangian Integrated Trajectory, Draxler and Rolph, 2003) backward trajectory calculation model has

255   been used. It has been run using the Global Data Assimilation System (GDAS) meteorological database and computing the back-trajectories for 48 hours prior to the arrival of air masses for the three stations at altitudes of 4700, 3700, and 2700 m asl (chosen based on the CAECENET results of Figure 6) on October 3rd at 10:00 UTC. The obtained back-trajectories are shown
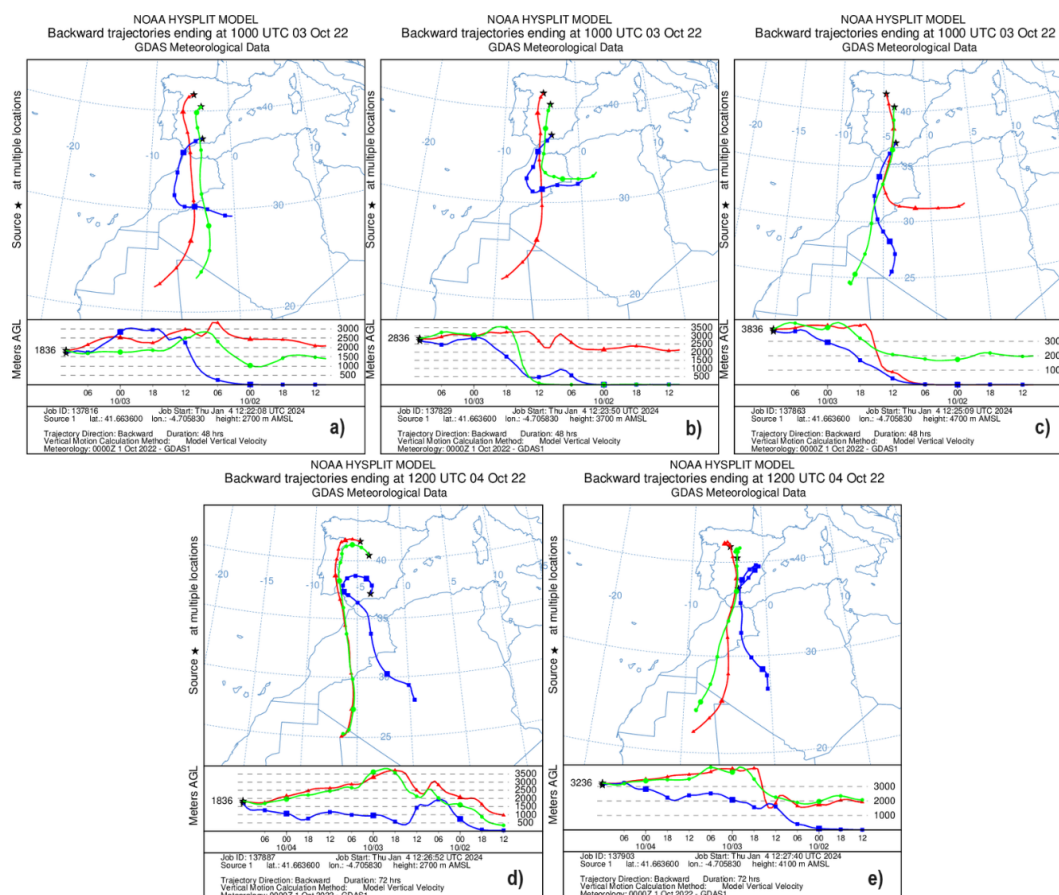
Figure 7. Back-trajectories from Valladolid, Madrid and Granada stations, calculated by HYSPLIT, at altitude levels of 2.7 km a), 3.7 km b) and 4.7 km asl c), on the 3rd October 10:00 UTC, and started at 2.7 km d) and 4.1 km asl e), on the 4th October 12:00 UTC.

in Figure 7, revealing that all back-trajectories come from the northern part of western Sahara. The air mass altitude was low on October 1st and 2nd and was elevated during its transport to the Iberian Peninsula. Although some trajectories are observed to deviate towards the east, the HYSPLIT ensemble mode has been also run (not shown here), confirming that the majority of trajectories originate from the same region. Only a few emerge from further to the east, more frequently in Granada than in Madrid and Valladolid. This could explain the differences in the volume concentration profiles. The back-trajectories for October 4th at 4100 and 2700 m asl are also shown in Figure 7 exhibiting a similar behavior: the air masses had their origin in the northwest region of the Sahara. Once again, in the case of Granada, the back-trajectory at 2700 m asl was deviated towards the east.

Once the aerosol origin has been identified, the NCEP/DOE meteorological reanalysis has been analyzed to characterize the synoptic situation. A surface-level low-pressure system began to form over the Sahara region on September 30th (not shown). This led to pump Saharan dust into the atmosphere. Additionally, on October 1st, a high-pressure system started to develop

at 700 hPa (about 3 km.) This anticyclone was responsible for the transport of the dust towards the Iberian Peninsula. This

270 scenario is referred to as NAH-A (North African High Located at Upper Levels) according to the classification of Escudero et al. (2005), and it is the most common pattern in the Peninsula between May and October (Cachorro et al., 2016). All these results confirm that the analyzed event was formed by Saharan mineral dust particles and explain the origin and transport mechanisms to reach the Iberian Peninsula at the observed heights in the CAECENET data.

3.2   Wildfire smoke event

275 In summer 2023 Canada suffered several forest fires that burned an estimated 18.4 million hectares (NASA, Earth Observatory, 2023). The intensity of the fires during June in the state of Quebec, resulted in the formation of a plume, generated by the extreme heat and convection triggered by the burning vegetation (Vaughan et al., 2018). Due to the predominant westerly winds prevalent at midlatitudes and the robust convection observed over Canada, which can lift smoke to high altitudes, even far above the planetary boundary layer, this plume could potentially travel long distances in accordance with local atmospheric

280 circulation patterns (Forster et al., 2001; Paugam et al., 2016). CAECENET network has enabled to monitor this long-range transport smoke event to the Iberian Peninsula.

Figure 8 shows the AOD and AE for the end of June 2023 at several CAECENET stations in the Iberian Peninsula. First, before noon on 26th, the AOD at 440 nm values at all stations were close to 0.2, not significantly above the average for those stations. Subsequently, a sharp increase was observed in Valladolid, reaching an AOD value at 440 nm of 1.47. The

285 following day, the values in Valladolid values remain high and an increase is early observed in Badajoz (AOD at 440 nm reaching 2.22), but also in Madrid (AOD at 440 nm up to 1.83) and Montsec (AOD at 440 nm about 0.56); this increase appeared in Granada at midday reaching AOD values at 440 nm close to 0.61. This increase in AOD was associated with AE values around 1.27, corresponding to predominant fine particles but with larger fine mode median size, due to coagulation and condensation processes during the large transport (Reid et al., 2005; Ditas et al., 2018). On 28 June, extreme values decrease

290 in Valladolid, Madrid, and Badajoz, but high AOD values still persist, indicative of a high-turbidity event across all stations, notably prominent in Montsec due to its elevated altitude and generally clean environment. Finally, on 29 June, lower AOD values began to recover at all stations, the AE showing different values among the stations.

Regarding the CAECENET columnar aerosol properties, the volume size distribution and the SSA values are shown in Figure 9 for June 27th. Volume size distribution showed a fine predominant mode, with a high peak in Valladolid, Madrid, and

295 Badajoz, reaching almost 0.2 μm^3/μm^2, centered around 0.2 μm. The retrieved fine modal radius for this day was 0.23 μm on average for all the stations, a typical value for aged smoke (Eck et al., 2009; González et al., 2020 b). In Montsec and Granada, the volume concentration for this day was lower because, as AOD has revealed, the highest aerosol load reached these stations one and two days after. The SSA values for Madrid and Badajoz exhibit a very similar trend, with a slight peak at 675 nm. In the case of Valladolid, a SSA decrease with the wavelength is observed, starting from 0.95 at 440 nm. In Granada values seem

300 constant around 0.91. These values are associated with smoke particles (Dubovik et al., 2002), and so, the AE values seen in Figure 8, therefore, the hypothesis that they may have been transported from the wildfires in Canada seems plausible.
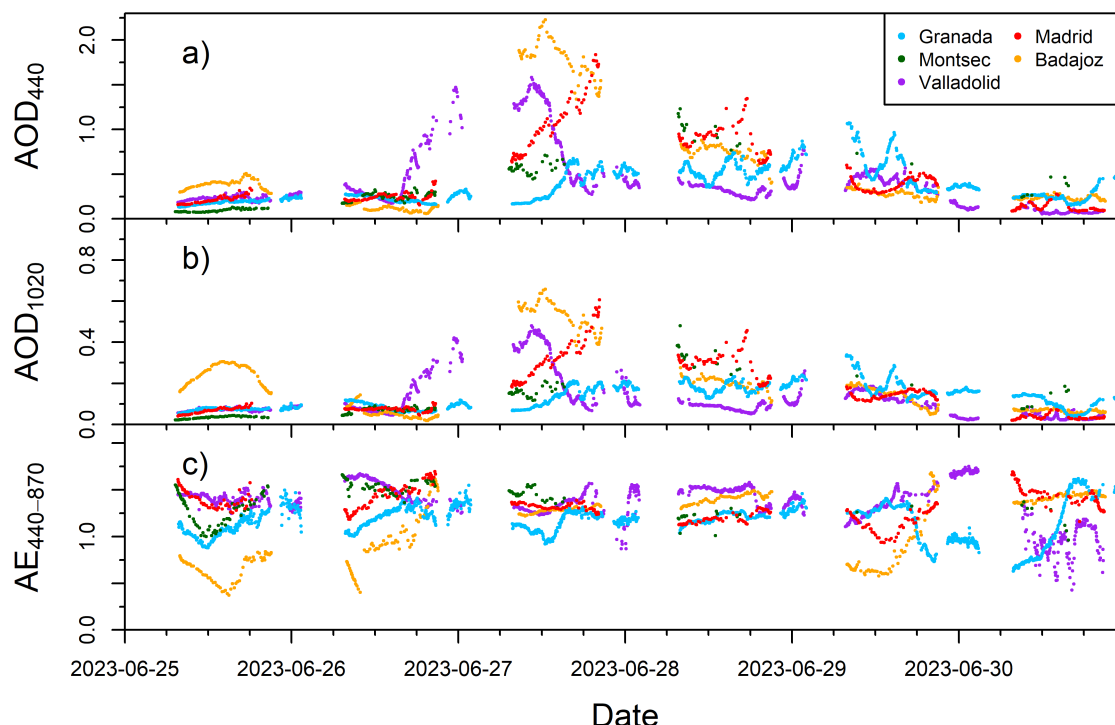
Figure 8. AOD values at 440 nm a), 1020 nm b), and Angström Exponent (AE) c), provided by CÆLIS (level 1.5), for Granada, Badajoz, Madrid, Montsec and Valladolid stations from June 25th to 30th, 2023.

It is possible to analyze the information in terms of altitude and track the evolution of the event through the ceilometer data from each station; in order to do so, the time series of the ceilometer RCS is plotted in Figure 10. It can be observed that an aerosol plume reached first Valladolid in the afternoon, followed by Madrid in the evening, and Badajoz and Montsec on late June 26th. The aerosol entered in two main thin layers around 5 and 8 km asl, which altitude was going quickly down to 3 and 5 km asl on June 27th, when the aerosol layers also come to Granada at midday. This event occurred in Montsec in the presence of clouds, which explain the scarcity of AOD data in this station.

Figure 11 shows the vertical volume concentration profiles provided by CAECENET for the days of the event. Only one retrieval is plotted in the graphs per day and station. The Valladolid VC profile on June 26th aligns well with the observed in Figure 10, showing a thin layer with a high aerosol volume concentration (up to 60 $\mu m^3/\mu m^2$) between 4 and 5 km asl and another wider layer at a higher altitude with lower concentration (about 20 $\mu m^3/\mu m^2$). In the rest of the stations on this day, there are no available inversions later, so high concentrations are not captured as the aerosol plume did not yet arrived, as seen in Figure 10. The following day, June 27th, the event is clearly observed at most of the stations. Madrid and Valladolid show similar profiles, with a concentration peak about 110 $\mu m^3/\mu m^2$, both peaks centered between 4 and 3 km asl respectively. Badajoz presents a similar peak than the mentioned for Valladolid but approximately 600 m below; this difference could be

15
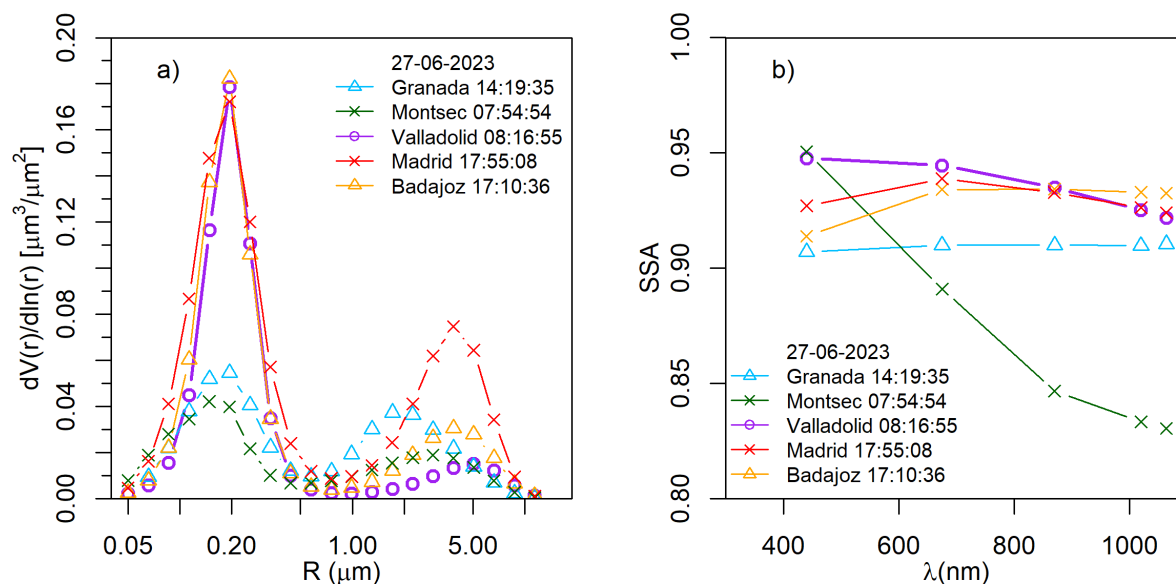
Figure 9. Size distribution a) and SSA b) obtained with $GRASP_{pac}$ and provided by CAECENET for the 27th of June, at UTC hours shown for each station.

caused by the orography, since the altitude of Valladolid is 520 m above Badajoz. Another peak in a wider layer around 5 km asl can be appreciated in some locations with lower VC values: about 60, 50 and 20 $\mu m^3/\mu m^2$ in Madrid, Valladolid and Badajoz, respectively. In Granada, a layer between 6 and 7 km asl appears that day with a maximum VC value of 20 $\mu m^3/\mu m^2$, which fits with the highest layer detected in Valladolid the day before. In Montsec, there are few available observations due to clouds, but the profile shown at 07:55 UTC in Figure 11, could indicate the presence of thin layers about 2 and 5 km asl.

On June 28th, a very pronounced VC peak about 140 $\mu m^3/\mu m^2$ appeared in Madrid in a thin layer around 3.2 km asl. In Valladolid on this day, a thin layer is also observed around 3.5 km asl but with lower VC values, being the peak below 40 $\mu m^3/\mu m^2$. In Granada, the aerosol plume was still remaining in high altitudes but in a broader layer (between 5.5 and 7 km asl), showing values close to 30 $\mu m^3/\mu m^2$. Finally, on June 29th, a layer around 4.5 km asl can be observed in Valladolid and Badajoz, with peak VC values between 30 and 20 $\mu m^3/\mu m^2$. Granada and Madrid presented the most intense layer around 4 and 3.5 km asl, respectively, with VC peak values between 60 and 50 $\mu m^3/\mu m^2$.

Regarding the vertical profiles of the extinction, scattering, absorption, and backscattering coefficients from the CAECENET inversions (shown in the appendix), the same pattern as in the vertical profile of volume concentration is observed. On 27th June, Valladolid and Madrid presented the highest values of the scattering coefficient at 440 nm, 891 Mm^{-1} and 661 Mm^{-1} respectively. In Badajoz, these values were slightly lower, measuring a peak of 503 Mm^{-1}. In Montsec, on 27th June, the scattering coefficient at the same wavelength reached values up to 123 Mm^{-1}. In Madrid, Valladolid and Badajoz, for the mentioned altitudes, the absorption coefficient at 440 nm reached a maximum of 53 Mm^{-1}, 34 Mm^{-1} and 39 Mm^{-1}, respectively.
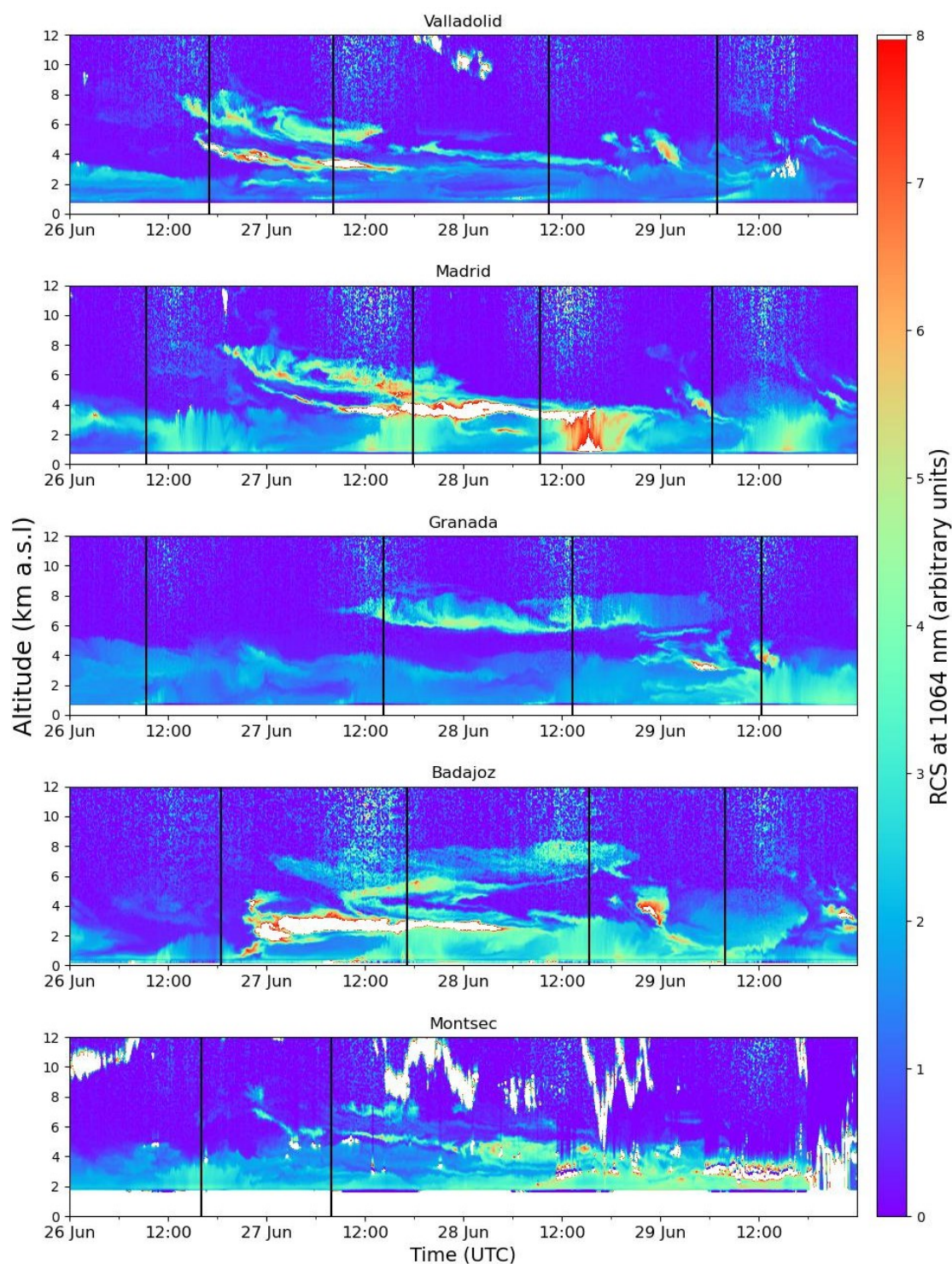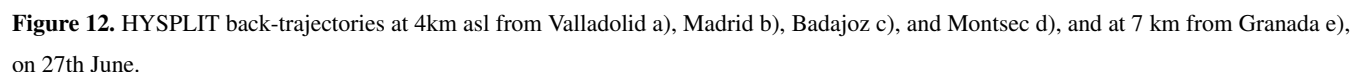
Figure 10. Ceilometer time series of range corrected signal representing the evolution of the event between 26th and 29th June 2023 at the stations of Valladolid (705 m), Madrid (669 m), Granada (680 m), Badajoz (186 m) and Montsec (1574 m). Black vertical lines indicate the time of the profiles in Figure 11 for each station.

17
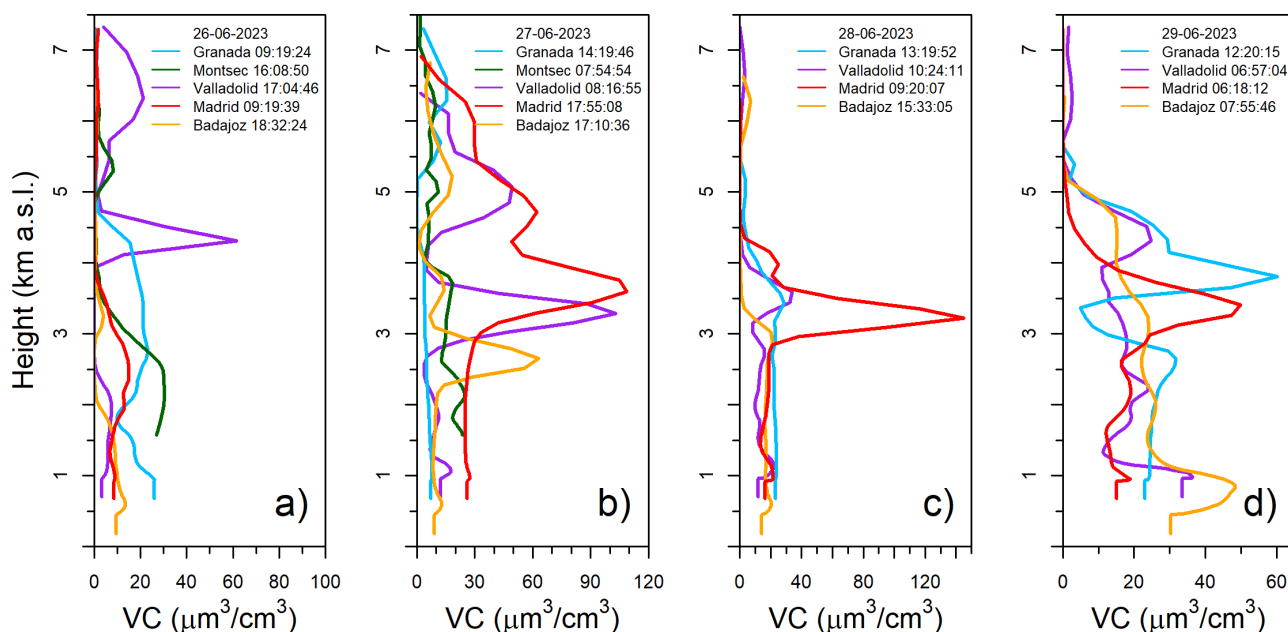
Figure 11. Volume concentration vertical profiles (altitudes from 0 to 8 km above sea level) at the studied stations. In panel a), the values are shown for June 26th, in panel b) for the 27th, panel c) for the 28th and panel d) for the 29th of June 2023, at the hours (UTC) indicated in the legend for each station.

The maximum absorption observed in Granada was around 7 Mm^{-1} for 440 nm. The backscattering coefficient at 440 nm presented the lowest values for Granada, under 1.1 Mm^{-1}sr^{-1}, in the case of Madrid and Badajoz, it gets values around 7.8

335 and 5.5 Mm^{-1}sr^{-1}, and up to 12.5 Mm^{-1}sr^{-1} for Valladolid. The extinction coefficient, agrees with the values mentioned for each coefficient, for 440 nm the highest values are found at Valladolid, around 940 Mm^{-1}, 714 and 517 Mm^{-1} for Madrid and Badajoz respectively and around 129 and 42 Mm^{-1} for Montsec and Granada.

Once the height of aerosol layers has been quantified, the HYSPLIT model has been run using ensemble mode to calculate the back-trajectories from the analyzed stations. These back-trajectories are shown in Figure 12 and they confirm that the

340 detected aerosol plume was transported from Canada, primarily from the region of Quebec. As shown in Figure 10, the aerosol plume was at a considerable altitude, above 6 km asl, and took between 5 and 6 days to reach the Iberian Peninsula. In the case of Montsec station (Figure 12 d)), the ensemble mode for trajectory calculation is presented to assess that air masses from the same region did reach the station. Therefore, even though there are not as many observations as in the other stations, it is possible to confirm that the event is the same. For Granada (Figure 12 e)), it is observed that despite the plume reached later,

345 its origin was the same. The NCEP/DOE reanalysis shows a strong high-pressure system extending from the surface to upper levels over the Atlantic Ocean. The northward location of the Azores anticyclone together with the position of the Icelandic low favoured westerly airflow carrying aerosol from the Canadian wildfires.

Figure 12. HYSPLIT back-trajectories at 4km asl from Valladolid a), Madrid b), Badajoz c), and Montsec d), and at 7 km from Granada e), on 27th June.

4   Conclusions

This work has introduced the CAECENET system, which aims to take advantage of the synergies between the data measured
350   by collocated sun-sky photometers and ceilometers using the GRASP code in the retrieval of both column and vertical aerosol
properties. The input data is obtained from CÆLIS and ICENET databases, and since both follow well-defined and well-known
measurement and calibration protocols, it is possible to automatically and continuously obtain these properties in near-real-time
in an accessible manner. This is very useful, for instance, in the analysis of regional aerosol events.

This study also presents the analysis of two aerosol events in the Iberian Peninsula. The first corresponds to a Saharan dust
355   outbreak that occurred between October 3rd and 5th, 2022. The analyzed data have shown that on October 3rd, aerosol optical
depth (AOD) at 400 increased up to values above 0.5 nm with Angström Exponent (AE) values below 0.2 in the Spanish
stations of Madrid, Valladolid, and Granada. The vertical profiles have revealed that the layer of mineral dust aerosols was
transported at around 3 km asl altitude, although in Granada, there was also aerosol load at surface level. On October 4th, the
aerosols descended in altitude, being gradually removed from the atmosphere on October 5th. The optical properties provided
360   by CAECENET fit with typical values for Saharan mineral dust particles, with SSA close to 1 except for 440 nm and very
low absorption coefficients. Back-trajectories analysis and meteorological data have indicated that this outbreak had the origin
source in the Sahara desert and it occurred due to the presence of a low-pressure system in this region, which pumped up the
dust in the surface, and subsequently, an anticyclone sited on North-Africa around 3 km asl in altitude, was responsible of the
aerosol transport to the Iberian Peninsula at this altitude.

365   The other event analyzed corresponds to the transport of particles from the Canadian wildfires in in June 2023. This event
has been observed in the Iberian Peninsula at Badajoz, Granada, Madrid, Montsec, and Valladolid sites, where unusually high
AOD values were measured between 26th and 29th June. Back-trajectories have confirmed that its origin was the wildfires in
the province of Quebec in Canada. The smoke particles were transported at high altitudes to reach the Iberian Peninsula, as
shown by the volume concentration profiles, with values exceeding 100 $\mu m^3/\mu m^2$. At the stations of Valladolid, Madrid, and
370   Badajoz, aerosol plumes have been observed at different altitudes, generally between 3 and 5 km asl.

Concluding, this work has demonstrated that CAECENET is an useful and powerful tool that can be used to monitor,
characterize and quantify vertically-resolved aerosol properties. In fact, CAECENET has been used before in various works
such as in the study of aerosol vertical radiative forcing (Bazo et al., 2023) or in the monitoring of volcanic plumes over the
Iberian Peninsula (Salgueiro et al., 2023). Furthermore, in near future, CAECENET could be configured to assimilate data
375   from other types of lidar systems, such as Micropulse Lidars (MPL), or from other ceilometer networks, like E-PROFILE, to
provide the GRASP$_{pac}$ products at a larger number of locations.

Appendix A: Vertical profiles of optical properties
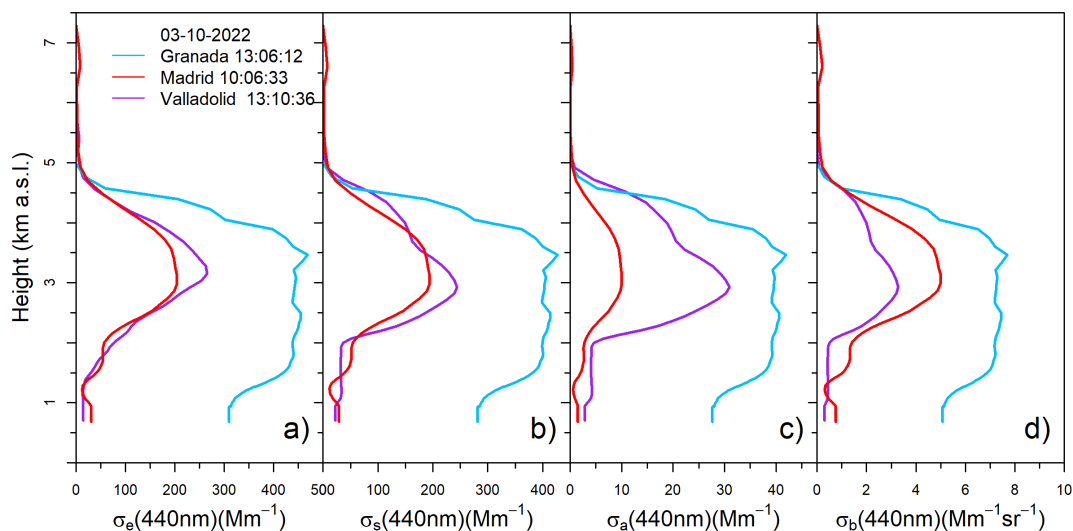
Figure A1. Vertical profiles (altitudes from 0 to 8 km above sea level) of extinction coefficient a), scattering coefficient b), absorption coefficient c) and backscattering coefficient d). For October 3rd 2022, at the hours (UTC) indicated in the legend for each station.
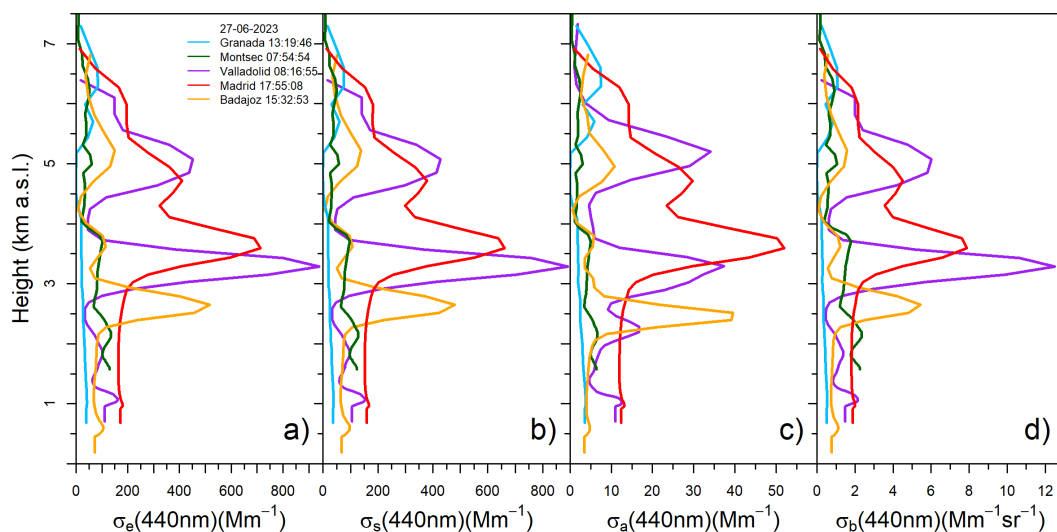
Figure A2. Vertical profiles (altitudes from 0 to 8 km above sea level) of extinction coefficient a), scattering coefficient b), absorption coefficient c) and backscattering coefficient d). For June 27th 2023, at the hours (UTC) indicated in the legend for each station.

References

Ansmann, A., Riebesell, M., and Weitkamp, C.: Measurement of atmospheric aerosol extinction profiles with a Raman lidar, Opt. Lett., 15, 746–748, https://doi.org/10.1364/OL.15.000746, 1990.

Barreto, A., Cuevas, E., Damiri, B., Guirado, C., Berkoff, T., Berjón, A. J., Hernández, Y., Almansa, F., and Gil, M.: A new method for nocturnal aerosol measurements with a lunar photometer prototype, Atmospheric Measurement Techniques, 6, 585–598, https://doi.org/10.5194/amt-6-585-2013, 2013.

Barreto, A., Cuevas, E., Granados-Muñoz, M.-J., Alados-Arboledas, L., Romero, P. M., Gröbner, J., Kouremeti, N., Almansa, A. F., Stone, T., Toledano, C., Román, R., Sorokin, M., Holben, B., Canini, M., and Yela, M.: The new sun-sky-lunar Cimel CE318-T multiband photometer – a comprehensive performance evaluation, Atmospheric Measurement Techniques, 9, 631–654, https://doi.org/10.5194/amt-9-631-2016, 2016.

Barreto, Á., Román, R., Cuevas Agulló, E., Berjón, A., Almansa Rodríguez, A. F., Toledano, C., González, R., Pérez, H., Yballa, C., Blarel, L., et al.: Assessment of nocturnal aerosol optical depth from lunar photometry at the Izaña high mountain observatory, Atmospheric Measurement Techniques, 10, 3007–3019, 2017.

Bazo, E., Granados-Muñoz, M. J., Román, R., Bravo-Aranda, J. A., Cazorla, A., Valenzuela, A., González, R., Olmo, F. J., and Alados-Arboledas, L.: Evaluation of the vertically-resolved aerosol radiative effect on shortwave and longwave ranges using sun-sky photometer and ceilometer measurements, Atmospheric Research, 282, 106 517, https://doi.org/https://doi.org/10.1016/j.atmosres.2022.106517, 2023.

Benavent-Oltra, J. A., Román, R., Granados-Muñoz, M. J., Pérez-Ramírez, D., Ortiz-Amezcua, P., Denjean, C., Lopatin, A., Lyamani, H., Torres, B., Guerrero-Rascado, J. L., Fuertes, D., Dubovik, O., Chaikovsky, A., Olmo, F. J., Mallet, M., and Alados-Arboledas, L.: Comparative assessment of GRASP algorithm for a dust event over Granada (Spain) during ChArMEx-ADRIMED 2013 campaign, Atmospheric Measurement Techniques, 10, 4439–4457, https://doi.org/10.5194/amt-10-4439-2017, 2017.

Benavent-Oltra, J. A., Román, R., Casquero-Vera, J. A., Pérez-Ramírez, D., Lyamani, H., Ortiz-Amezcua, P., Bedoya-Velásquez, A. E., de Arruda Moreira, G., Barreto, A., Lopatin, A., Fuertes, D., Herrera, M., Torres, B., Dubovik, O., Guerrero-Rascado, J. L., Goloub, P., Olmo-Reyes, F. J., and Alados-Arboledas, L.: Different strategies to retrieve aerosol properties at night-time with the GRASP algorithm, Atmospheric Chemistry and Physics, 19, 14 149–14 171, https://doi.org/10.5194/acp-19-14149-2019, 2019.

Burgos, M., Mateos, D., Cachorro, V., Toledano, C., and de Frutos, A.: Aerosol properties of mineral dust and its mixtures in a regional background of north-central Iberian Peninsula, Science of The Total Environment, 572, 1005–1019, https://doi.org/https://doi.org/10.1016/j.scitotenv.2016.08.001, 2016.

Cachorro, V., Casanova, J., and de Frutos, A.: The influence of ångström parameters on calculated direct solar spectral irradiances at high turbidity, Solar Energy, 39, 399–407, https://doi.org/https://doi.org/10.1016/S0038-092X(87)80058-0, 1987.

Cachorro, V. E., Burgos, M. A., Mateos, D., Toledano, C., Bennouna, Y., Torres, B., de Frutos, A. M., and Herguedas, A.: Inventory of African desert dust events in the north-central Iberian Peninsula in 2003–2014 based on sun-photometer–AERONET and particulate-mass–EMEP data, Atmospheric Chemistry and Physics, 16, 8227–8248, https://doi.org/10.5194/acp-16-8227-2016, 2016.

Cazorla, A., Casquero-Vera, J. A., Román, R., Guerrero-Rascado, J. L., Toledano, C., Cachorro, V. E., Orza, J. A. G., Cancillo, M. L., Serrano, A., Titos, G., Pandolfi, M., Alastuey, A., Hanrieder, N., and Alados-Arboledas, L.: Near-real-time processing of a ceilometer network assisted with sun-photometer data: monitoring a dust outbreak over the Iberian Peninsula, Atmospheric Chemistry and Physics, 17, 11 861–11 876, https://doi.org/10.5194/acp-17-11861-2017, 2017.

Chen, C., Dubovik, O., Fuertes, D., Litvinov, P., Lapyonok, T., Lopatin, A., Ducos, F., Derimian, Y., Herman, M., Tanré, D., Remer, L. A., Lyapustin, A., Sayer, A. M., Levy, R. C., Hsu, N. C., Descloitres, J., Li, L., Torres, B., Karol, Y., Herrera, M., Herreras, M., Aspets-
430   berger, M., Wanzenboeck, M., Bindreiter, L., Marth, D., Hangler, A., and Federspiel, C.: Validation of GRASP algorithm product from POLDER/PARASOL data and assessment of multi-angular polarimetry potential for aerosol monitoring, Earth System Science Data, 12, 3573–3620, https://doi.org/10.5194/essd-12-3573-2020, 2020.

Ditas, J., Ma, N., Zhang, Y., Assmann, D., Neumaier, M., Riede, H., Karu, E., Williams, J., Scharffe, D., Wang, Q., Saturno, J., Schwarz, J. P., Katich, J. M., McMeeking, G. R., Zahn, A., Hermann, M., Brenninkmeijer, C. A. M., Andreae, M. O., Pöschl, U., Su, H., and Cheng,
435   Y.: Strong impact of wildfires on the abundance and aging of black carbon in the lowermost stratosphere, Proceedings of the National Academy of Sciences, 115, E11 595–E11 603, https://doi.org/10.1073/pnas.1806868115, 2018.

Draxler, R. and Rolph, G.: HYSPLIT (HYbrid Single-Particle Lagrangian Integrated Trajectory) Model access via NOAA ARL READY Website (http://www.arl.noaa.gov/ready/hysplit4.html), Tech. rep., NOAA, 2003.

Dubovik, O. and King, M.: A Flexible Inversion Algorithm for Retrieval of Aerosol Optical Properties from Sun and Sky Radiance Mea-
440   surements., J. Geophys. Res., 105, 20,673–20,696, 2000.

Dubovik, O., Smirnov, A., Holben, B. N., King, M. D., Kaufman, Y. J., Eck, T. F., and Slutsker, I.: Accuracy assessments of aerosol optical properties retrieved from Aerosol Robotic Network (AERONET) Sun and sky radiance measurements, Journal of Geophysical Research, 105, 9791–9806, 2000.

Dubovik, O., Holben, B., Eck, T., Smirnov, A., Kaufman, Y., King, M. D., Tanre, D., and Slutsker, I.: Variability of Absorption and Optical
445   Properties of Key Aerosol Types Observed in Worldwide Locations, Journal of the Atmospheric Sciences, 59, 590–608, 2002.

Dubovik, O., Sinyuk, A., Lapyonok, T., Holben, B. N., Mishchenko, M., Yang, P., Eck, T. F., Volten, H., Muñoz, O., Veihelmann, B., van der Zande, W. J., Léon, J.-F., Sorokin, M., and Slutsker, I.: Application of spheroid models to account for aerosol particle nonsphericity in remote sensing of desert dust, Journal of Geophysical Research, 111, D11 208, https://doi.org/doi:10.1029/2005JD006619, 2006.

Dubovik, O., Lapyonok, T., Litvinov, P., Herman, M., Fuertes, D., Ducos, F., Lopatin, A., Chaikovsky, A., Torres, B., Derimian, Y.,
450   Huang, X., Aspetsberger, M., and Federspiel, C.: GRASP: a versatile algorithm for characterizing the atmosphere, SPIE: Newsroom, https://doi.org/doi:10.1117/2.1201408.005558, 2014.

Dubovik, O., Fuertes, D., Litvinov, P., Lopatin, A., Lapyonok, T., Doubovik, I., Xu, F., Ducos, F., Chen, C., Torres, B., Derimian, Y., Li, L., Herreras-Giralda, M., Herrera, M., Karol, Y., Matar, C., Schuster, G. L., Espinosa, R., Puthukkudy, A., Li, Z., Fischer, J., Preusker, R., Cuesta, J., Kreuter, A., Cede, A., Aspetsberger, M., Marth, D., Bindreiter, L., Hangler, A., Lanzinger, V., Holter, C., and Federspiel, C.: A
455   Comprehensive Description of Multi-Term LSM for Applying Multiple a Priori Constraints in Problems of Atmospheric Remote Sensing: GRASP Algorithm, Concept, and Applications, 2 (2021), http://dx.doi.org/10.17169/refubium-36696, 2021.

Eck, T. F., Holben, B. N., Reid, J. S., Sinyuk, A., Hyer, E. J., O'Neill, N. T., Shaw, G. E., Vande Castle, J. R., Chapin, F. S., Dubovik, O., Smirnov, A., Vermote, E., Schafer, J. S., Giles, D., Slutsker, I., Sorokine, M., and Newcomb, W. W.: Optical properties of boreal region biomass burning aerosols in central Alaska and seasonal variation of aerosol optical depth at an Arctic coastal site, Journal of Geophysical
460   Research: Atmospheres, 114, https://doi.org/https://doi.org/10.1029/2008JD010870, 2009.

Escudero, M., Castillo, S., Querol, X., Avila, A., Alarcon, M., Viana, M. M., Alastuey, A., Cuevasn, E., , and Rodriguez, S.: Wet and dry African dust episodes over eastern Spain, J. Geophys. Res., 110, D18S08, 2005.

Espinosa, W. R., Remer, L. A., Dubovik, O., Ziemba, L., Beyersdorf, A., Orozco, D., Schuster, G., Lapyonok, T., Fuertes, D., and Martins, J. V.: Retrievals of aerosol optical and microphysical properties from Imaging Polar Nephelometer scattering measurements, Atmospheric
465   Measurement Techniques, 10, 811–824, https://doi.org/10.5194/amt-10-811-2017, 2017.

Fernald, F. G.: Analysis of atmospheric lidar observations: some comments, Appl. Opt., 23, 652–653, https://doi.org/10.1364/AO.23.000652, 1984.

Forster, C., Wandinger, U., Wotawa, G., James, P., Mattis, I., Althausen, D., Simmonds, P., O'Doherty, S., Jennings, S. G., Kleefeld, C., Schneider, J., Trickl, T., Kreipl, S., Jäger, H., and Stohl, A.: Transport of boreal forest fire emissions from Canada to Europe, Journal of Geophysical Research: Atmospheres, 106, 22 887–22 906, https://doi.org/https://doi.org/10.1029/2001JD900115, 2001.

Fuertes, D., Toledano, C., González, R., Berjón, A., Torres, B., Cachorro, V. E., and de Frutos, A. M.: CÆLIS: software for assimilation, management and processing data of an atmospheric measurement network, Geoscientific Instrumentation, Methods and Data Systems, 7, 67–81, https://doi.org/10.5194/gi-7-67-2018, 2018.

Giles, D. M., Sinyuk, A., Sorokin, M. G., Schafer, J. S., Smirnov, A., Slutsker, I., Eck, T. F., Holben, B. N., Lewis, J. R., Campbell, J. R., Welton, E. J., Korkin, S. V., and Lyapustin, A. I.: Advancements in the Aerosol Robotic Network (AERONET) Version 3 database – automated near-real-time quality control algorithm with improved cloud screening for Sun photometer aerosol optical depth (AOD) measurements, Atmospheric Measurement Techniques, 12, 169–209, https://doi.org/10.5194/amt-12-169-2019, 2019.

González, R., Toledano, C., Román, R., Fuertes, D., Berjón, A., Mateos, D., Guirado-Fuentes, C., Velasco-Merino, C., Antuña-Sánchez, J. C., Calle, A., Cachorro, V. E., and de Frutos, A. M.: Daytime and nighttime aerosol optical depth implementation in CÆLIS, Geoscientific Instrumentation, Methods and Data Systems, 9, 417–433, https://doi.org/10.5194/gi-9-417-2020, 2020 a.

González, R., Toledano, C., Román, R., Mateos, D., Asmi, E., Rodríguez, E., Lau, I. C., Ferrara, J., D'Elia, R., Antuña-Sánchez, J. C., Cachorro, V. E., Calle, A., and de Frutos, M.: Characterization of Stratospheric Smoke Particles over the Antarctica by Remote Sensing Instruments, Remote Sensing, 12, https://doi.org/10.3390/rs12223769, 2020 b.

Guerrero-Rascado, J. L., Sicard, M., Molero, F., Navas-Guzmán, F., Preißler, J., Kumar, D., Bravo-Aranda, J. A., Tomás, S., Reba, M. N., Alados-Arboledas, L., Comerón, A., Pujadas, M., Rocadenbosch, F., and Silva, F. W. A. M.: Monitoring of the Eyjafjalla Volcanic Plume at Four Lidar Stations over the Iberian Peninsula: 6 to 8 May 2010, IV Reunión Espa̅Â¿Â½ola de Ciencia y Tecnología del aerosol – RECTA, 2010.

Herrera, M. E., Dubovik, O., Torres, B., Lapyonok, T., Fuertes, D., Lopatin, A., Litvinov, P., Chen, C., Benavent-Oltra, J. A., Bali, J. L., and Ristori, P. R.: Estimates of remote sensing retrieval errors by the GRASP algorithm: application to ground-based observations, concept and validation, Atmospheric Measurement Techniques, 15, 6075–6126, https://doi.org/10.5194/amt-15-6075-2022, 2022.

Herreras, M., Román, R., Cazorla, A., Toledano, C., Lyamani, H., Torres, B., Cachorro, V., Olmo, F., Alados-Arboledas, L., and de Frutos, A.: Evaluation of retrieved aerosol extinction profiles using as reference the aerosol optical depth differences between various heights, Atmospheric Research, 230, 104 625, https://doi.org/https://doi.org/10.1016/j.atmosres.2019.104625, 2019.

Herrero-Anta, S., Román, R., Mateos, D., González, R., Antuña Sánchez, J. C., Herreras-Giralda, M., Almansa, A. F., González-Fernández, D., Herrero del Barrio, C., Toledano, C., Cachorro, V. E., and de Frutos, A. M.: Retrieval of aerosol properties from zenith sky radiance measurements, EGUsphere, 2023, 1–29, https://doi.org/10.5194/egusphere-2023-1040, 2023.

Holben, B. N., Eck, T. F., Slutsker, I., Tanré, D., Buis, J. P., Setzer, A., Vermote, E., Reagan, J. A., Kaufman, Y. J., Nakajima, T., Lavenu, F., Jankowiak, I., and Smirnov, A.: AERONET – a federated instrument network and data archive for aerosol characterization, Remote Sens. Environ., 66, 1–16, 1998.

Klett, J. D.: Stable analytical inversion solution for processing lidar returns, Appl. Opt., 20, 211–220, https://doi.org/10.1364/AO.20.000211, 1981.

Klett, J. D.: Lidar inversion with variable backscatter/extinction ratios, Appl. Opt., 24, 1638–1643, https://doi.org/10.1364/AO.24.001638, 1985.

Li, X. and Strahler, A.: Geometric-optical bidirectional reflectance modeling of the discrete crown vegetation canopy: effect of crown shape
505   and mutual shadowing, IEEE Transactions on Geoscience and Remote Sensing, 30, 276–292, https://doi.org/10.1109/36.134078, 1992.

Lopatin, A., Dubovik, O., Chaikovsky, A., Goloub, P., Lapyonok, T., Tanré, D., and Litvinov, P.: Enhancement of aerosol characterization
    using synergy of lidar and sun-photometer coincident observations: the GARRLiC algorithm, Atmospheric Measurement Techniques, 6,
    2065–2088, https://doi.org/10.5194/amt-6-2065-2013, 2013.

Lopatin, A., Dubovik, O., Fuertes, D., Stenchikov, G., Lapyonok, T., Veselovskii, I., Wienhold, F. G., Shevchenko, I., Hu, Q., and Parajuli, S.:
510   Synergy processing of diverse ground-based remote sensing and in situ data using the GRASP algorithm: applications to radiometer, lidar
    and radiosonde observations, Atmospheric Measurement Techniques, 14, 2575–2614, https://doi.org/10.5194/amt-14-2575-2021, 2021.

Mateos, D., Cachorro, V., Toledano, C., Burgos, M., Bennouna, Y., Torres, B., Fuertes, D., González, R., Guirado, C., Calle, A., and de Frutos,
    A.: Columnar and surface aerosol load over the Iberian Peninsula establishing annual cycles, trends, and relationships in five geographical
    sectors, Science of The Total Environment, 518-519, 378–392, https://doi.org/https://doi.org/10.1016/j.scitotenv.2015.03.002, 2015.

515 Molero, F., Pujadas, M., and Artíñano, B.: Study of the Effect of Aerosol Vertical Profile on Microphysical Properties Using GRASP Code
    with Sun/Sky Photometer and Multiwavelength Lidar Measurements, Remote Sensing, 12, https://doi.org/10.3390/rs12244072, 2020.

NASA, Earth Observatory: Tracking Canada's Extreme 2023 Fire Season, https://earthobservatory.nasa.gov/images/151985/
    tracking-canadas-extreme-2023-fire-season#:~:text=Ignited%20by%20lightning%20on%20June,and%20drought%20gripped%20the%
    20region., 2023.

520 Pappalardo, G., Amodeo, A., Apituley, A., Comeron, A., Freudenthaler, V., Linné, H., Ansmann, A., Bösenberg, J., D'Amico, G., Mattis, I.,
    Mona, L., Wandinger, U., Amiridis, V., Alados-Arboledas, L., Nicolae, D., and Wiegner, M.: EARLINET: towards an advanced sustainable
    European aerosol lidar network, Atmospheric Measurement Techniques, 7, 2389–2409, https://doi.org/10.5194/amt-7-2389-2014, 2014.

Paugam, R., Wooster, M., Freitas, S., and Val Martin, M.: A review of approaches to estimate wildfire plume injection height within large-
    scale atmospheric chemical transport models, Atmospheric Chemistry and Physics, 16, 907–925, https://doi.org/10.5194/acp-16-907-
525   2016, 2016.

Reid, J. S., Koppmann, R., Eck, T. F., and Eleuterio, D. P.: A review of biomass burning emissions part II: intensive physical properties of
    biomass burning particles, Atmospheric Chemistry and Physics, 5, 799–825, https://doi.org/10.5194/acp-5-799-2005, 2005.

Román, R., Benavent-Oltra, J. A., Casquero-Vera, J. A., Lopatin, A., Cazorla, A., Lyamani, H., Denjean, C., Fuertes, D., Pérez-Ramírez,
    D., Torres, B., et al.: Retrieval of aerosol profiles combining sunphotometer and ceilometer measurements in GRASP code, Atmospheric
530   Research, 204, 161–177, 2018.

Román, R., González, R., Cazorla, A., Herreras-Giralda, M., Antuña-Sánchez, J., and Toledano, C.: CAECENET: Columnar and Vertically-
    Resolved Aerosol Products in near-Real-Time joining Sun/Sky Photometer and Ceilometer Measurement Networks, in: European Lidar
    Conference, vol. 5, Granada, 2021.

Román, R., Antuña Sánchez, J. C., Cachorro, V. E., Toledano, C., Torres, B., Mateos, D., Fuertes, D., López, C., González, R., Lapionok, T.,
535   Herreras-Giralda, M., Dubovik, O., and de Frutos, A. M.: Retrieval of aerosol properties using relative radiance measurements from an
    all-sky camera, Atmospheric Measurement Techniques, 15, 407–433, https://doi.org/10.5194/amt-15-407-2022, 2022.

Román, R., Torres, B., Fuertes, D., Cachorro, V., Dubovik, O., Toledano, C., Cazorla, A., Barreto, A., Bosch, J., Lapyonok, T., González,
    R., Goloub, P., Perrone, M., Olmo, F., de Frutos, A., and Alados-Arboledas, L.: Remote sensing of lunar aureole with a sky camera:
    Adding information in the nocturnal retrieval of aerosol properties with GRASP code, Remote Sensing of Environment, 196, 238–252,
540   https://doi.org/https://doi.org/10.1016/j.rse.2017.05.013, 2017.

Román, R., González, R., Toledano, C., Barreto, A., Pérez-Ramírez, D., Benavent-Oltra, J. A., Olmo, F. J., Cachorro, V. E., Alados-Arboledas, L., and de Frutos, A. M.: Correction of a lunar-irradiance model for aerosol optical depth retrieval and comparison with a star photometer, Atmospheric Measurement Techniques, 13, 6293–6310, https://doi.org/10.5194/amt-13-6293-2020, 2020.

Ross, I. and Ross, J.: The radiation regime and architecture of plant stands, 3, Springer Science & Business Media, 1981.

545   Salgueiro, V., Guerrero-Rascado, J., Costa, M., Román, R., Cazorla, A., Serrano, A., Molero, F., Sicard, M., Córdoba-Jabonero, C., Bortoli, D., Comerón, A., Couto, F., López-Cayuela, M., Pérez-Ramírez, D., Potes, M., Muñiz-Rosado, J., Obregón, M., Barragán, R., Oliveira, D., Abril-Gago, J., González, R., Gíl-Díaz, C., Foyo-Moreno, I., Muñoz-Porcar, C., Granados-Muñoz, M., Rodríguez-Gómez, A., Herreras-Giralda, M., Bravo-Aranda, J., Carvajal-Pérez, C., Barreto, A., and Alados-Arboledas, L.: Characterization of Tajogaite volcanic plumes detected over the Iberian Peninsula from a set of satellite and ground-based remote sensing instrumentation, Remote Sensing of Environment, 295, 113 684, https://doi.org/https://doi.org/10.1016/j.rse.2023.113684, 2023.

Sasano, Y. and Nakane, H.: Significance of the extinction/backscatter ratio and the boundary value term in the solution for the two-component lidar equation, Appl. Opt., 23, $11_1 - -13$, https://doi.org/$10.1364/AO.23.0011\_1$, 1984.

Sinyuk, A., Holben, B. N., Eck, T. F., Giles, D. M., Slutsker, I., Korkin, S., Schafer, J. S., Smirnov, A., Sorokin, M., and Lyapustin, A.: The AERONET Version 3 aerosol retrieval algorithm, associated uncertainties and comparisons to Version 2, Atmospheric Measurement Techniques, 13, 3375–3411, https://doi.org/10.5194/amt-13-3375-2020, 2020.

Titos, G., Ealo, M., Román, R., Cazorla, A., Sola, Y., Dubovik, O., Alastuey, A., and Pandolfi, M.: Retrieval of aerosol properties from ceilometer and photometer measurements: long-term evaluation with in situ data and statistical analysis at Montsec (southern Pyrenees), Atmospheric Measurement Techniques, 12, 3255–3267, https://doi.org/10.5194/amt-12-3255-2019, 2019.

Toledano, C., Cachorro, V. E., Berjon, A., de Frutos, A. M., Sorribas, M., de la Morena, B. A., and Goloub, P.: Aerosol optical depth and Angstrom exponent climatology at El Arenosillo AERONET site (Huelva, Spain), Quarterly Journal of the Royal Meteorological Society, 133, 795–807, https://doi.org/Doi 10.102/Qj.54, 2007.

560 Torres, B. and Fuertes, D.: Characterization of aerosol size properties from measurements of spectral optical depth: a global validation of the GRASP-AOD code using long-term AERONET data, Atmospheric Measurement Techniques, 14, 4471–4506, https://doi.org/10.5194/amt-14-4471-2021, 2021.

Torres, B., Dubovik, O., Fuertes, D., Schuster, G., Cachorro, V. E., Lapyonok, T., Goloub, P., Blarel, L., Barreto, A., Mallet, M., Toledano, C., and Tanré, D.: Advanced characterisation of aerosol size properties from measurements of spectral optical depth using the GRASP algorithm, Atmospheric Measurement Techniques, 10, 3743–3781, https://doi.org/10.5194/amt-10-3743-2017, 2017.

Tsekeri, A., Lopatin, A., Amiridis, V., Marinou, E., Igloffstein, J., Siomos, N., Solomos, S., Kokkalis, P., Engelmann, R., Baars, H., Gratsea, M., Raptis, P. I., Binietoglou, I., Mihalopoulos, N., Kalivitis, N., Kouvarakis, G., Bartsotas, N., Kallos, G., Basart, S., Schuettemeyer, D., Wandinger, U., Ansmann, A., Chaikovsky, A. P., and Dubovik, O.: GARRLiC and LIRIC: strengths and limitations for the characterization of dust and marine particles along with their mixtures, Atmospheric Measurement Techniques, 10, 4995–5016, https://doi.org/10.5194/amt-10-4995-2017, 2017.

Valenzuela, A., Olmo, F., Lyamani, H., Antón, M., Titos, G., Cazorla, A., and Alados-Arboledas, L.: Aerosol scattering and absorption Angström exponents as indicators of dust and dust-free days over Granada (Spain), Atmospheric Research, 154, 1–13, https://doi.org/https://doi.org/10.1016/j.atmosres.2014.10.015, 2015.

Vaughan, G., Draude, A. P., Ricketts, H. M. A., Schultz, D. M., Adam, M., Sugier, J., and Wareing, D. P.: Transport of Canadian forest fire smoke over the UK as observed by lidar, Atmospheric Chemistry and Physics, 18, 11 375–11 388, https://doi.org/10.5194/acp-18-11375-2018, 2018.

Wei, Y., Li, Z., Zhang, Y., Chen, C., Xie, Y., Lv, Y., and Dubovik, O.: Derivation of PM10 mass concentration from advanced satellite retrieval products based on a semi-empirical physical approach, Remote Sensing of Environment, 256, 112 319, https://doi.org/https://doi.org/10.1016/j.rse.2021.112319, 2021.

Whiteman, D. N., Melfi, S. H., and Ferrare, R. A.: Raman lidar system for the measurement of water vapor and aerosols in the Earth's atmo-
580   sphere, Appl. Opt., 31, 3068–3082, https://doi.org/10.1364/AO.31.003068, 1992.